Intramolecular Dimerization Quenching of Delayed Emission in Asymmetric D−D′−A TADF Emitters

Kai-Lin Woon,[*,†,‡] Chih-Lun Yi,[§] Kuan-Chung Pan,[⊥] Marc K. Etherington,[†] Chung-Chih Wu,[*,⊥] Ken-Tsung Wong,[*,§,∥] and Andrew P. Monkman[*,†]

†Department of Physics, Durham University, South Road, Durham DH1 3LE, U.K.

‡Low Dimensional Materials Research Centre, Department of Physics, University of Malaya, Kuala Lumpur 50603, Malaysia

§Department of Chemistry, National Taiwan University, No. 1, Sec. 4, Roosevelt Road, Taipei 10617, Taiwan

∥Institute of Atomic and Molecular Science, Academia Sinica, Taipei 10617, Taiwan

⊥Department of Electrical Engineering, Graduate Institute of Electronics Engineering, and Graduate Institute of Photonics and Optoelectronics, National Taiwan University, Taipei 10617, Taiwan

S *Supporting Information*

ABSTRACT: Understanding the excited-state dynamics and conformational relaxation in thermally activated delayed fluorescence (TADF) molecules, including conformations that potentially support intramolecular through-space charge transfer, can open new avenues for TADF molecular design as well as elucidate complex photophysical pathways in structurally complex molecules. Emissive molecules comprising a donor (triphenylamine, TPA) and an acceptor (triphenyltriazine, TRZ) bridged by a second donor (9,9-dimethyl-9-10-dihydroacridin, DMAC, or phenoxazine, PXZ)

are synthesized and characterized. In solution, the flexibility of the sp³-hybridized carbon atom in DMAC of **DMAC−TPA−TRZ**, compared to the rigid PXZ, allows significant conformational reorganization, giving rise to multiple charge-transfer excited states. As a result of such a reorganization, the TRZ and TPA moieties become cofacially aligned, driven by a strong dipole−dipole attraction between the TPA and TRZ units, forming a weakly charge-transfer dimer state, in stark contrast to the case of **PXZ−TPA−TRZ** where the rigid PXZ bridge only supports a single PXZ−TRZ charge transfer (CT) state. The low-energy TPA-TRZ dimer is found to have a high-energy dimer local triplet state, which quenches delayed emission because the resultant singlet CT local triplet energy gap is too large to mediate efficient reverse intersystem crossing. However, organic light-emitting diodes using **PXZ−TPA−TRZ** as an emitting dopant resulted in external quantum efficiency as high as 22%, more than two times higher than that of **DMAC−TPA−TRZ**-based device, showing the impact that such intramolecular reorganization and donor−acceptor dimerization have on TADF performance.
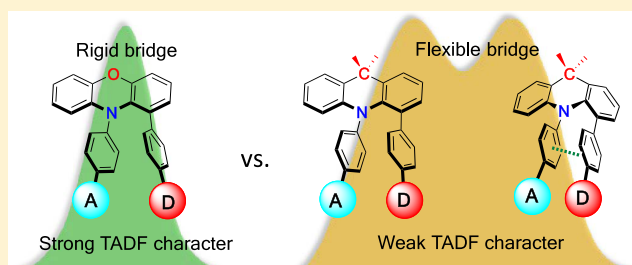
1. INTRODUCTION

Organic molecules that yield thermally activated delayed fluorescence (TADF) have evolved to become the third-generation materials for organic light-emitting diodes (OLEDs).[1] Unlike phosphorescent emitters, TADF molecules can harvest triplet excitons by a reverse intersystem crossing (rISC) mechanism between the triplet charge-transfer states (³CT) and the singlet charge-transfer states (¹CT) mediated by vibronic coupling between ³CT and a local excited triplet state (³LE) when the energy gap between all three states becomes small, <100 meV.[2−4] One of the key parameters in achieving extremely small singlet−triplet splitting (ΔE_{ST}) is the use of conformational twisting between donor (D) and acceptor (A) to minimize the overlap between the highest occupied molecular orbital (HOMO) and the lowest unoccupied molecular orbital (LUMO).[5−7] Beyond the subtle manipulations on the degree of intramolecular through-bond charge transfer, recent interest in through-space charge transfer between D and A moieties, mediated by strong intramolecular π−π dipolar interactions between D and A, has been motivated by the potential of increasing the photoluminescence quantum yield.[8,9] In a conjugated system, the D and A can be arranged cofacially, in close proximity, using a noncoplanar molecular scaffold.[10] This approach has also led to the design of nonconjugated polymers with spatially separated pendant D and A.[11,12] Despite the growing interest of intramolecular through-space charge transfer as a means to TADF, there have been few detailed studies of the excited-state dynamics and molecular conformations of such systems. Here, we investigate the excited-state dynamics of new molecules configured with asymmetrical donor−donor′−acceptor (D−D′−A) architectures, where the electron-donor (D) moiety (triphenylamine,
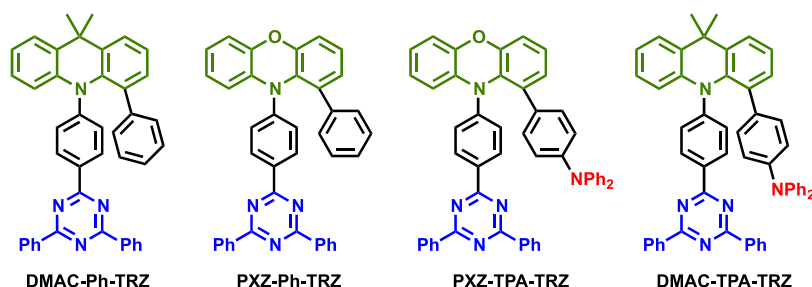
Figure 1. Chemical structures of the TADF molecules studied.
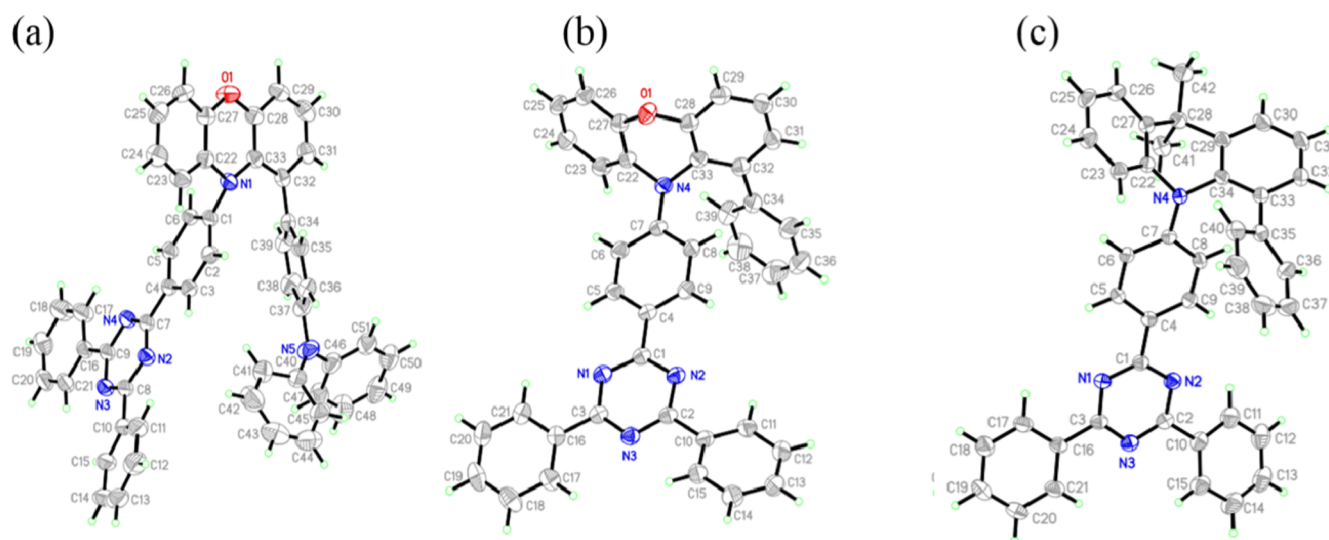

Figure 2. Molecular structures of (a) **PXZ−TPA−TRZ**, (b) **PXZ−Ph−TRZ**, and (c) **DMAC−Ph−TRZ** with thermal ellipsoids drawn at a 50% probability level.

TPA) is bridged through a donor' (D') such as 9,9-dimethyl-9-10-dihydroacridin (DMAC) or phenoxazine (PXZ) to link to the electron acceptor (A) (triphenyltriazine, TRZ). The former is referred to as **DMAC−TPA−TRZ** and the latter is **PXZ−TPA−TRZ**, as shown in Figure 1. Both DMAC and PXZ moieties are popular electron-donating groups that are used to construct high-performance TADF emitters.[13−18] In a previous study of a linear D−A−D′ system, the near orthogonality of both D and D′ units separated by the A ensured strong decoupling of the electrons on the D and A in the CT state.[19] In this study, the secondary donor TPA and TRZ acceptor are placed in close proximity, which allows us to investigate the detailed excited-state dynamics in the presence of potential through-space D/A interactions. Here, we observe that **DMAC−TPA−TRZ** exhibits multiple CT states, one of which, between TPA and TRZ, is mediated by strong dipole−dipole coupling between the D and A, which drives an activated cofacially intramolecular dimerization, giving through-space charge transfer resulting in an excited-state intramolecular dimeric CT state. However, we find that this low-energy CT state has a high-energy dimer local triplet state that introduces a large singlet−triplet gap that effectively quenches rISC. In sharp contrast, this type of D/A interaction does not occur in **PXZ−TPA−TRZ**, which was rationalized as a result of the rigidity of the bridging PXZ moiety.

2. RESULTS AND DISCUSSION

The synthesis of target molecules **PXZ−TPA−TRZ** and **DMAC−TPA−TRZ** is shown in Scheme S1, and the detailed procedures and characterization of all materials are reported in the Supporting Information (SI). To probe the excited states of these complex systems, we replaced triphenylamine (TPA) with a phenyl group (Ph) to make further two compounds, **PXZ−Ph−TRZ** and **DMAC−Ph−TRZ** (Figure 1), which were synthesized from intermediates PXZ−Ph and DMAC−Ph.[20] All of the newly synthesized molecules were purified by column chromatography followed by vacuum sublimation before characterization and device fabrication. Single crystals of **PXZ−TPA−TRZ**, **PXZ−Ph−TRZ**, and **DMAC−Ph−TRZ** suitable for X-ray diffraction analysis were obtained by a bilayer (CH$_2$Cl$_2$/hexane) diffusion method. Unfortunately, a single crystal of **DMAC−TPA−TRZ** could not be obtained. Figure 2 depicts the single crystal structures of **PXZ−TPA−TRZ**, **PXZ−Ph−TRZ**, and **DMAC−Ph−TRZ**. Full crystallographic data are summarized in Table S1 in the SI and Figure S1. Ortho-substituted donors of TADF molecules commonly exhibit folded conformations because of the large steric interaction between the ortho-substituted group and acceptor.[21,22] The folded conformation in the electron-donating moiety was also observed in **PXZ−Ph−TRZ** and **DMAC−Ph−TRZ**. The X-ray structures of **PXZ−Ph−TRZ** and **DMAC−Ph−TRZ** (Figure 2) indicate buckled conformations of the donating units PXZ and DMAC. The PXZ of **PXZ−Ph−TRZ** and DMAC of **DMAC−Ph−TRZ** exhibit a distorted boat configuration and are folded relative to the phenylene bridge plane, creating dihedral angles of 115.4 and 127.2°, respectively. In addition, the dihedral angles between the phenyl group and its donor of **PXZ−Ph−TRZ** and **DMAC−**
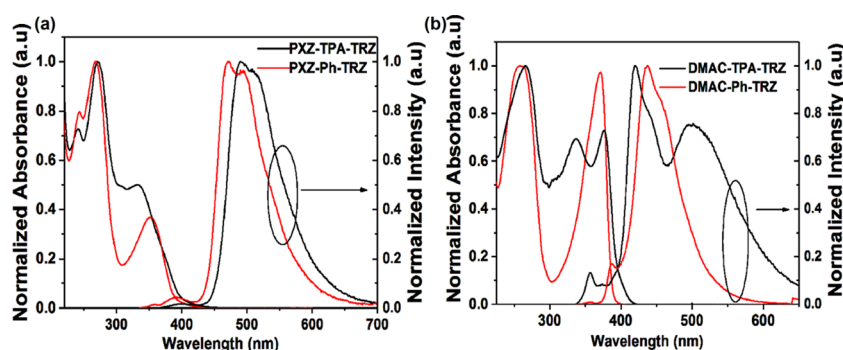
Figure 3. UV−vis and PL spectra of 10 μg mL^{-1} in MCH solution of (a) **PXZ−TPA−TRZ** and **PXZ−Ph−TRZ**, and (b) **DMAC−TPA−TRZ** and **DMAC−Ph−TRZ**.
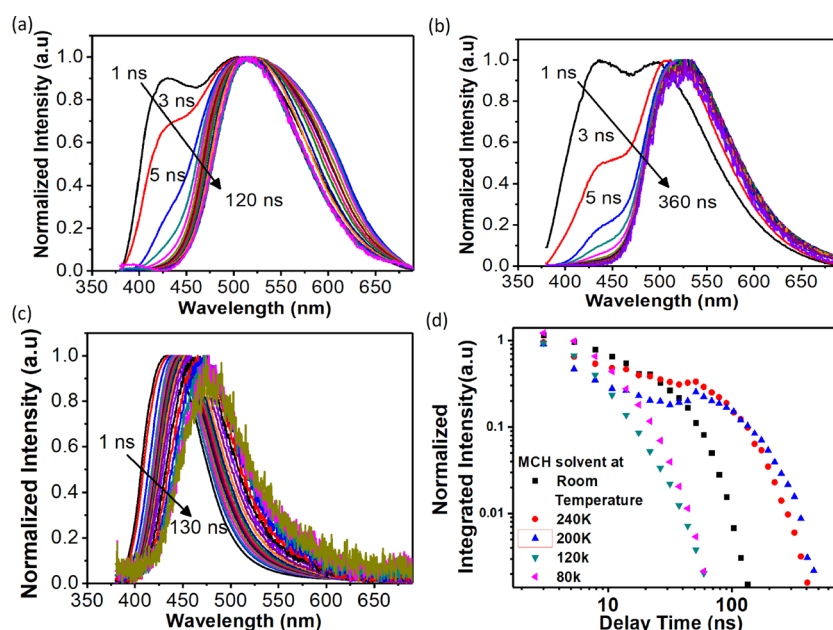

Figure 4. Time evolution of the spectral shape of **DMAC−TPA−TRZ** in MCH (a) at room temperature, (b) at 240 K, and (c) 120 K (frozen). Notice the disappearance of the second peak when the solution is frozen. (d) Normalized integrated intensity at different temperatures.

Ph−TRZ are calculated to be 41.4 and 53.0°, respectively. As observed in the **PXZ−Ph−TRZ** and **DMAC−Ph−TRZ** crystals, the boat configuration leads to a highly twisted D−A configuration, where the nitrogen lone-pair electrons of the donor unit align favorably for better π-conjugation with the TRZ rather than with the phenylene ring of the donor unit. Thus, the N−C (TRZ) bond in **PXZ−Ph−TRZ** and **DMAC−Ph−TRZ** is shorter than the N−C (PXZ and DMAC) bond, whereas the N−C (TRZ) bond in **PXZ−TPA−TRZ** is longer than the N−C (PXZ) bond, as indicated in Figure 2. In the **PXZ−TPA−TRZ** case, the buckled conformation of the PXZ unit is not observed by X-ray analysis. Instead, the central ring of PXZ in **PXZ−TPA−TRZ** is practically planar and exhibits a highly twisted D−A conformation with a dihedral angle of 75.6° between PXZ and TRZ core (Figure S1). The TRZ lies in a quasi-equatorial configuration[23,24] with respect to the PXZ, with the N−C bridging bond tilted by ∼36.5° with respect to the PXZ plane, resulting in the staggered arrangement of TPA and TRZ at a shortened C−N distance of 2.931 Å. In addition, the dihedral angle between the triphenylamine and PXZ of **PXZ−TPA−TRZ** is calculated to be 57.6°.

Figure 3a shows the normalized absorption and emission spectra of **PXZ−TPA−TRZ** and **PXZ−Ph−TRZ** in methylcyclohexane (MCH). Optical transitions at ∼270 and ∼350 nm can be attributed to the TRZ and PXZ moieties, respectively, while TPA exhibits an absorption peak at ∼320 nm. The emission spectra of both **PXZ−Ph−TPZ** and **PXZ−TPA−TRZ** are similar except the latter is red-shifted. Figure 3b depicts the normalized absorption and emission spectra of **DMAC−TPA−TRZ** and **DMAC−Ph−TRZ** in MCH. Both absorption edges of **PXZ−TPA−TRZ** and **DMAC−TPA−TRZ** are red-shifted with respect to TPA-free molecules, indicating increased conjugation in the π system of PXZ and DMAC (Figure S2). The emission spectra of each material in nonpolar MCH reveal a slightly structured band, suggesting a mixed locally excited (^{1}LE) and ^{1}CT character of the state. The increase in photoluminescence (PL) intensity in degassed solvents (Figure S3) indicates a contribution from the triplet states (Table S2). In polar solvents such as toluene, the emission loses all its structure, indicative of an increased CT character. A strong positive solvatochromic shift of the onset of emission band in polar solvents indicates strong CT character of the transition. The shift of the emission-onset energy for each material between MCH and toluene is largest in **PXZ−**
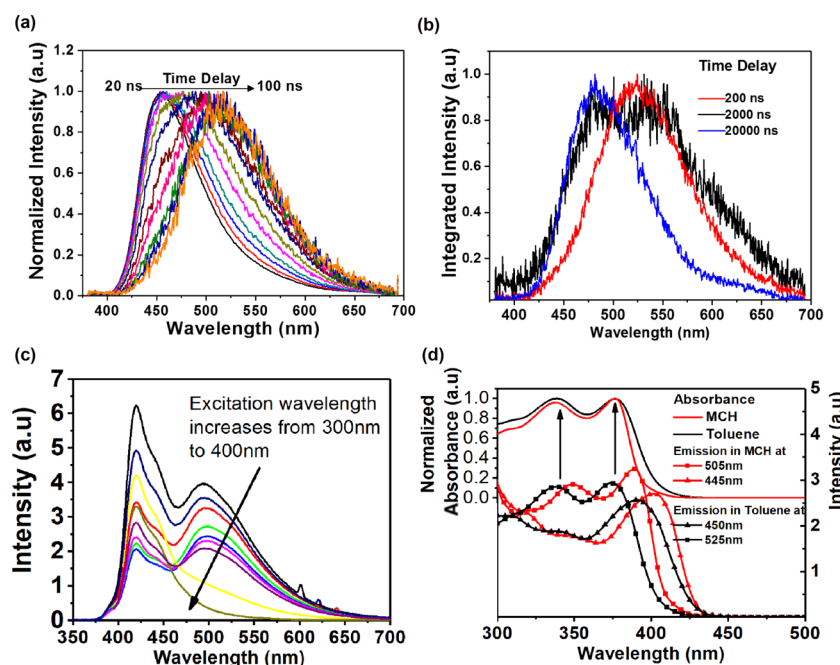
Figure 5. Time-resolved spectra of (a) PF and (b) DF of **DMAC−TPA−TRZ** at room temperature in zeonex matrix. (c) PL spectra with different excitation wavelengths in MCH and (d) photoluminescence excitation (PLE) and overlay with absorption curve in MCH and toluene.

Ph−TRZ (0.19 eV), followed by **PXZ−TPA−TRZ** (0.14 eV) and then by **DMAC−TPA−TRZ** (0.11 eV) with **DMAC−Ph−TRZ** showing the smallest shift (0.06 eV). Incorporating TPA in **PXZ−Ph−TRZ** decreases the induced change in dipole moment (degree of charge transfer) compared to that in **PXZ−Ph−TRZ**, indicating a stronger stabilization of the charge transfer in **PXZ−TPA−TRZ** in a nonpolar environment. However, it increases the degree of charge-transfer character significantly for **DMAC−TPA−TRZ**. **DMAC−Ph−TRZ** is seen to have the weakest CT character supported by it having the smallest integrated intensity ratio between degassed and aerated solvent in MCH, which only increases slightly in toluene (Table S2). Interestingly, in MCH, **DMAC−TPA−TRZ** singularly exhibits two very distinct emission bands centered at 420 and 525 nm. In toluene, the 525 nm band red-shifts only slightly but the intensity is greatly reduced, indicative of a CT state with a near-complete one-electron transfer from D to A, whereas the emission centered at 420 nm red-shifts far more, compared to its position in MCH concomitant with weak CT in MCH. **DMAC−Ph−TRZ** in comparison shows this larger red shift of its single band from 430 nm in MCH to 480 nm, indicating stabilization of the DMAC−TRZ CT state with polarity.[25] From this, we make an initial identification of the two CT states in **DMAC−TPA−TRZ** to be a DMAC−TRZ CT state at 420 nm and a TPA−TRZ CT state at 525 nm (taking the MCH data). The weak emission band between 350 and 400 nm is ascribed to donor [1]LE emission of the DMAC/PXZ moieties, which are initially excited with 325 nm (Figure S4).

To elucidate the nature of the **DMAC−TPA−TRZ** dual emission, time-resolved fluorescence spectroscopy in MCH was carried out using time-gated emission measurements using an iCCD-based spectrometer having a time resolution better than 1 ns.[1] At room temperature, the spectrum is complex. The blue band at ca. 425 nm decays very rapidly, within 10 ns, as shown in Figure 4a. This band is neither D nor A emission (see Figure S5), confirming it most likely to be a DMAC−TRZ CT

state. The short lifetime indicating it being quenched by intramolecular energy transfer to the lower-energy CT state. Inspection of the lower-energy emission band indicates the presence of two emitting CT components, centered at ca. 485 nm and ca. 575 nm, both being present from very early times. The 485 nm component red-shifts over the first 200 ns, reaching 525 nm. The lowest-energy CT band has a much shorter lifetime and shows little or no red shift either in time or with increasing solvent polarity, Figure S3. By deduction, we assigned this lowest-energy state to arise from the TPA−TRZ D A pair but having weak CT character. At 240 and 200 K in Figure 4b (and Figure S6), this lowest-energy TPA−TRZ species is not observed. Further, cooling the MCH solution below its freezing point suppresses the green 575 nm emission completely and hinders the formation of the 485 nm CT state, as seen in Figure 4c. Given that the low-energy excited states are not observed at low temperature, the lack of quenching of the 425 nm band at low temperatures indicates that the formation of these low-energy bands requires thermal activation. This would be in line with excited states that form after the large geometric reorganization of the molecule.[26]

The disappearance of the lowest-energy TPA−TRZ species component coincides with the appearance of DF in the time-resolved emission of **DMAC−TPA−TRZ** (Figure 4d). At room temperature, the decay curve is single exponential, while at 240 and 200 K, DF is also observed. The spectra observed at 120 K, Figure 4c, are very similar to those found in **DMAC−Ph−TRZ**, Figure S8, at early times, indicative of the DMAC−TRZ early-time CT state. In frozen solution, it is clear that this state relaxes very slowly, red-shifting over 0.25 eV in 200 ns. This may indicate that this state can relax into another state but the bulky substitution on the DMAC and the confinement in the frozen solution make this process very slow indeed.

Comparing this behavior to our previously reported[27,28] dual emission from axial and equatorial D−A conformations, we propose that the fast decay blue band at 425 nm could be

evidence for an axial DMAC−TRZ conformation that is rapidly quenched by the lower-energy TPA−TRZ states.[29]

In zeonex matrix, the lower-energy emission components of **DMAC−TPA−TRZ** are suppressed as they are in frozen solution (Figure S7), having an integrated emission band very similar to that observed in frozen MCH, indicating that large molecular reorganization is required to form these emissive species. However, the prompt fluorescence during the first few 100 ns (PF) of **DMAC−TPA−TRZ** in zeonex shows two clear emitting species, one centered at ca. 450 nm and the second at 510 nm, as shown in Figure 5a. The lowest-energy feature has a fast lifetime of only a few hundred nanoseconds, whereas the higher-energy component gives longtime DF but with significantly reduced intensity. This again points to the lowest-energy TPA−TRZ band having a different character to the higher-energy component.

The CT bands of **PXZ−TPA−TRZ** and **DMAC−Ph−TPZ** in zeonex display an apparent spectral shift of ca. 0.12 eV over 100 ns, whereas **PXZ−Ph−TPZ** shows no spectral shift in time at all (Figure S8). This spectral shift is, however, an effect of D−A dihedral angle heterogeneity giving large lifetime dispersion of the CT emission.[30,31] The higher-energy CT states decay faster than the lower-energy species due to their increased LE character, giving an apparent time-dependent spectral shift. The lack of emission shift in **PXZ−Ph−TPZ** demonstrates that it has a very rigid structure that narrows the structural inhomogeneity. This rigidity can be traced back to the large steric interaction between the phenyl group and the donor. The apparent spectral shifts in the **DMAC−Ph−TRZ** are larger than those in **PXZ−Ph−TRZ**, implying greater flexibility of the DMAC moiety. The presence of apparent spectral shift over time for **PXZ−TPA−TRZ** also implies the presence of structural inhomogeneity in a disordered medium. In **DMAC−TPA−TRZ**, we observe a similar shift in the 485 nm band (MCH) at early times but not the 575 nm band, indicating that the latter has far less heterogeneity and a more rigid configuration. The very large shift of the DMAC−TRZ CT band in frozen solution may indicate very large heterogeneity in this molecule in frozen solution, whereas the TPA−TRZ CT band shows little or no such heterogeneity, Figures 5a and S6, indicating a much more rigid and well-defined state.

DMAC−TPA−TRZ in zeonex again shows multiple distinct CT emissions occurring on different time scales, as illustrated in Figure 5b. The prompt emission shows an initial 450 nm band that decays within 50 ns, leaving a low-energy feature centered at 510 nm. This low-energy band does appear to grow in as the high-energy feature decays, again indicating that the species giving rise to the 450 nm band is quenched by the species yielding the 510 nm band. The delayed fluorescence, Figure 5b, clearly shows two distinct low-energy emissive species, the 510 nm band decaying in microseconds, leaving a band at 480 nm. The emission at 2 μs is the superposition of two bands, but at 200 ns, there is no emission at 480 nm, which may indicate that the low-energy species converts to the higher-energy species which then emits at 480 nm.

The CT bands of **DMAC−TPA−TRZ** are found to be excitation-energy-dependent, but counterintuitively, the low-energy CT emission bands disappear as the excitation energy decreases, Figure 5c. Surprisingly, lower-energy excitation gives rise only to the higher-energy blue emission, whereas the lower-energy green emission component requires excitation at higher energy. Such behavior is observed in MCH, toluene,

and 2-methyltetrahydrofuran solutions (Figure S9). This indicates that these low-energy species require excess energy to overcome a formation energy barrier. This then explains their greatly reduced contribution in solid zeonex. Photo-luminescence excitation (PLE) spectra from **DMAC−TPA−TRZ**, monitoring the emissions at 445 and 505 nm in MCH and at 450 and 525 nm in toluene were measured. These wavelengths correspond to the peak emission of each band in the respective solvent. Figure 5d shows this PLE and the absorbance of **DMAC−TPA−TRZ** in both solvents. The absorbance edge red-shifted with increasing solvent polarity from MCH to toluene while the locations of the peak absorbance are the same. The PLE curves for the blue and green components are very different. The PLE of the green component follows the shape of the absorbance, whereas the blue emission has a red-shifted PLE spectrum in both solvents. The PLE for all other materials (Figure S10) follows the absorbance curves almost exactly. The PLE of both components in **DMAC−TPA−TRZ** is red-shifted in MCH compared to that in toluene, consistent with the absorbance spectra, indicative of strong n−π* character. From the shape and position of the blue component PLE, which is located at the lower energy side of the absorbance, we assume that it arises from a direct CT absorption, i.e., from an n−π* transition.[30]

We performed a theoretical conformer search and found that **DMAC−TPA−TRZ** exists in two distinct conformational groups, having either a distorted boat or a planar DMAC configuration. Within the distorted boat configuration, the separation between TPA and TRZ is larger than the planar configuration (Figure S11). Both distorted and planar conformations exist in almost the same proportion, as their Gibbs free energies are the same. For **PXZ−TPA−TRZ**, the next lowest conformational structure of **PXZ−TPA−TRZ** differs by 0.6 kcal mol^{-1}, corresponding to a larger separation between TPA and TRZ. We believe that such conformational structures exist in an amorphous host medium, as evidenced in the time-resolved photoluminescence spectroscopy (Figure S8a)

Figure 5a shows the possible ground-state conformations for **DMAC−TPA−TRZ** optimized by density functional theory (DFT) using a tuned range-separated LC-ωPBE* functional at cc-pVDZ basis set level (Figure S12). This tuned range-separated LC-ωPBE* functional is used to minimize local-ization/delocalization error for CT states and was found to be a better predictor for vertical excitation (VE) energy of the singlet state ($E_{VE}(S_1)$) for CT molecules despite the fact that it tends to overestimate $E_{VE}(S_1)$;[32,33] for conformer 1 (Figure 6a), the TRZ is quasi-equatorial with respect to the DMAC,[24,34] with θ_t tilted by 34° with respect to the DMAC plane, while the tilting angle for TPA is less than 5° in the opposite direction as if TPA and TRZ are cofacially "skewed" away from each other. Conformer 1 has a continuous conjugation, while conformer 2, which is distorted, has a bending angle of 138°. Furthermore, for conformer 2, the TRZ is quasi-axial with respect to the DMAC[24,32] with TRZ and TPA "forked" away from each other with TRZ "pointing" downward by an angle of 68°. The interchromophic distance between TPA and TRZ is far shorter in conformer 1 than 2 with $d_1 = 3.28$ Å, $d_2 = 5.62$ Å (conformer 2) and $d_1 = 2.89$ Å, $d_2 = 4.56$ Å (conformer 1). Figure 6b shows the HOMO and LUMO levels of conformers 1 and 2 of **DMAC−TPA−TRZ**. One distinct difference is that there is no continuous electron
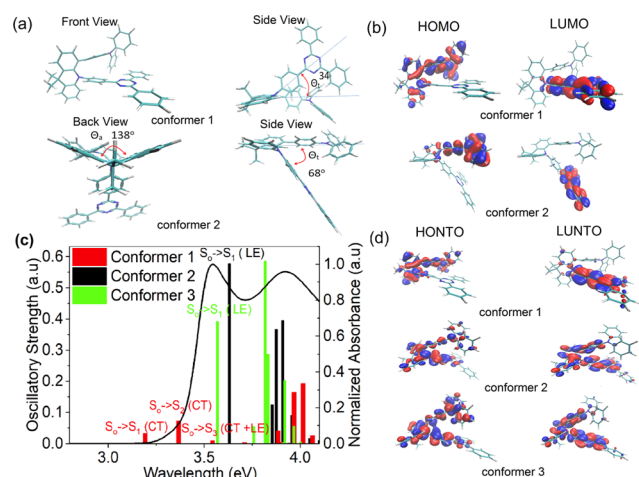
Figure 6. (a) DFT-optimized ground-state geometry of **DMAC–TPA–TRZ** conformers, (b) frontier orbitals of corresponding conformers, (c) calculated vertical excitation energy and respective oscillator strength for different conformers reduced by 0.25 eV overlaying with the absorption curve of **DMAC–TPA–TRZ** in MCH, and (d) HONTO and LUNTO of the lowest vertical excitation singlet states for different conformers.

delocalization for the HOMO level for the case of distorted DMAC. Unlike the LUMO levels of conformer 1, the N–C bridging bond in TRZ is not involved in the frontier orbitals in conformer 2, having a strong effect on the reverse intersystem crossing (rISC). Figure 6c shows the calculated singlet vertical excitation energy $E_{VE}(S_1)$ along with the oscillatory strength of the different conformers, reduced by 0.25 eV from the vacuum values, estimated using the Tamm–Dancoff approximation on time-dependent DFT at the LC-ωPBE*/cc-pVDZ level. Conformer 1 having a flat DMAC contributes significantly to CT states, which correspond to the absorption band edge states, while the first absorbance peak is mainly contributed by the distorted DMAC (conformer 2 and conformer 3).

Conformer 3 is a variant of conformer 2 with a smaller interchromophic distance between the TRZ and TPA. Natural transition orbitals (NTOs) are used to shed additional light on absorption and emission.[35] The corresponding NTOs for the five lowest-energy states are given in Figure 6d. For conformer 1, the highest occupied natural transition orbital (HONTO) and the lowest unoccupied natural transition orbital (LUNTO) are clearly dominated by the transition between HOMO and LUMO, in contrast with conformer 2 where the VE transition is not a CT state. If the TPA and TRZ are closer, as in conformer 3, the contribution from the frontier orbitals of the TPA increases, resulting in a red shift in the ^{1}LE state.

From Figure 6, it is clear that the ^{1}CT state, coming from conformer 1, results in the emission band at ~450 nm, whereas excitation in the ^{1}LE states of conformer 2 results in the ^{1}CT-like emission band at ~500 nm with a large Stoke shift, indicating pronounced geometric distortion in the excited adiabatic geometry. The question then arises, how does the vertical excitation of the lowest ^{1}LE state transform into the lowest-energy emissive state of the system having a geometric distortion?

To elucidate this transformation, we mixed equal amounts of TPA and TRZ (units) by weight in toluene. We observed a new emission band occurring at ~500 nm, not present in pure solutions of either molecule, which decreased in intensity with decreasing concentration, as shown in Figure 7a, indicating emission from a TPA/TRZ excited-state complex. Normally, exciplexes do not readily form in solution as the intermolecular distance is large compared to the solid state.[36] The formation of a TPA/TRZ complex in solution thus indicates a high stabilization energy[37−39] between TPA and TRZ. The emission peak also shifts with increasing solvent polarity, indicating a state with large excited-state dipole moment (Figure S13). Interestingly, whereas the emission from TPA is completely suppressed in chloroform, diluting a mixture of TPA/TRZ to 10 μg mL^{-1} in chloroform has no effect in suppressing the complex emission, suggesting that very strong stabilization can
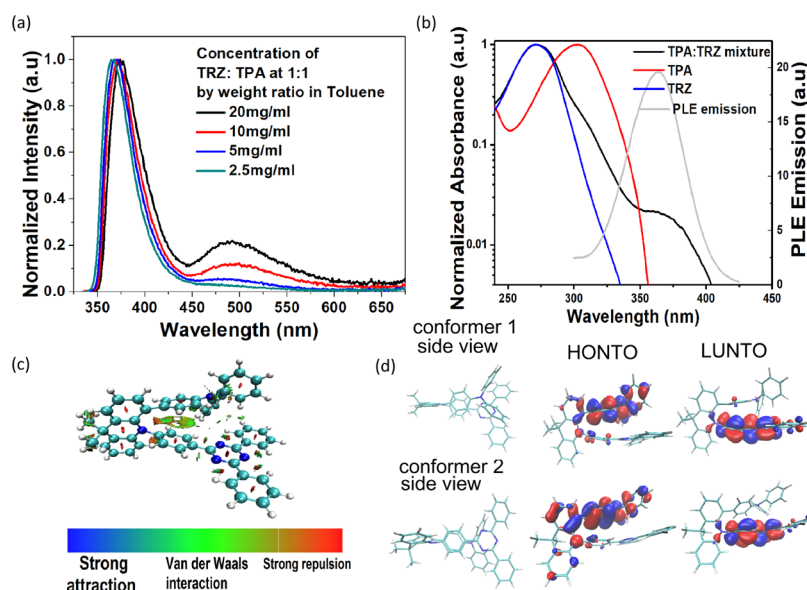

Figure 7. (a) PL of TPA/TRZ mixture in toluene with different concentrations, (b) PLE and absorption of the dilute mixture in chloroform, (c) reduced density gradient mapping for conformer 1 of **DMAC–TPA–TRZ** at ground state, (d) optimized excited geometries with d_1 = 2.81 Å, d_2 = 3.73 Å in conformer 2 of **DMAC–TPA–TRZ** along with their HONTO and LUNTO as compared to those of conformer 1 for vertical fluorescence.

be conferred in chloroform. We also measured the PLE and absorption of the diluted TPA/TRZ mixture. The absorption curve is not a superposition of the absorption curves of TPA and TRZ; rather, a new absorption band appeared at 350−400 nm, peaking at 365 nm, corresponding to the maximum PLE emission, as illustrated in Figure 7b. This indicates that the interaction between TPA and TRZ occurs in the ground state, i.e., a physical heterodimer state, not an exciplex.[40]

This shows the strong possibility of such an interaction between the TPA and TRZ in **DMAC−TPA−TRZ** and **PXZ−TPA−TRZ** if enough geometric rearrangement can occur in the molecule. Given that this state is only observed in **DMAC−TPA−TRZ** where the DMAC can be distorted to allow large geometric rearrangement and that frozen solution or a solid host matrix severely hinder the formation of this state, we can now ascribe the lowest emissive state in **DMAC−TPA−TRZ** as an intramolecular TPA−TRZ dimer, having partial CT character.

Noncovalent interactions can be used to visualize such an interaction in three-dimensional real space using a reduced density gradient, as shown in Figure 7c.[41,42] It is clear that there is a van der Waals interaction between the connecting aromatic rings of TPA and TRZ to the DMAC. The same behavior can be seen in **PXZ−TPA−TRZ** with the interaction strength reduced when the TPA and TRZ are further away from each other (Figure S14). Minimizing the excited-state geometry of conformers 1 and 2 of **DMAC−TPA−TRZ** gives a completely different geometry with respect to the ground state. The θ_t is reduced from 34° at ground state (Figure 6a) to 7.6° at the adiabatic geometry for conformer 1, while θ_t changes from 68° to less than 1° in conformer 2. In conformer 2, the TPA and TRZ moieties become cofacial with each other, as shown in Figure 7d. The large screwing motion for conformer 2, to bring TPA and TRZ to be cofacial with each other, results in the large Stoke shift in emission and dimerization forming new emission band at lower energy. The HONTO and LUNTO are now located predominantly at TPA and TRZ, respectively.

Figure 8a shows the optimized ground-state geometry of **PXZ−TPA−TRZ**. The arrangement of TPA and TRZ is very similar to conformer 1 of **DMAC−TPA−TRZ**, including the frontier electron distribution. However, the TPA and TRZ

moieties are not cofacial in the adiabatic excited-state geometry, as shown in Figure 8b, and the θ_t is reduced from 56 to 15°. We rationalized this through the rigidity of the PXZ moiety. The HONTO and LUNTO now located on PXZ and TRZ, respectively, as if TPA does not participate in the CT emission. Although the HOMO and LUMO of **DMAC−Ph−TRZ** and **PXZ−Ph−TRZ** are spatially separated (Figure S15), from the NTO, the vertical fluorescence state of **DMAC−Ph−TRZ** shows strong mixing of [1]LE state, hence reducing its CT character, as seen in Figure 8c. This is consistent with the small energy onset shift in **DMAC−Ph−TRZ** observed between MCH and toluene, an indicative of a strong [1]LE character. This is expected to increase the electron exchange energy, introducing a larger energy gap between [3]CT and [3]LE, while **PXZ−Ph−TPZ** shows a clear CT character (Figure 8d) and it is expected to have a small energy gap.[2]

To correlate these theoretical results with the molecular photophysics and TADF behavior, time-resolved emission measurements at room temperature in zeonex were again carried out, as shown in Figure 9a. Both **PXZ−TPA−TRZ** and **PXZ−Ph−TRZ** display clear transition from prompt to DF emission at ∼100 ns with the prompt emission having two decay lifetimes of 2.93 ns ([1]LE from donor) and 7.83 ns ([1]CT) for **PXZ−TPA−TRZ** and a single prompt exponential decay of 11.6 ns ([1]CT) for **PXZ−Ph−TRZ**, while the delay CT lifetimes are 10.6 and 7.99 μs for **PXZ−TPA−TRZ** and **PXZ−Ph−TRZ**, respectively (Figures S16 and S17). This is not surprising as their ΔE_{ST} are very small ∼0.03 eV or less. The rISC rates for **PXZ−TPA−TRZ** and **PXZ−Ph−TRZ** are determined[5] to be 7.64×10^4 and 1.48×10^5 s^{-1}, respectively (Table S3). However, **DMAC−TPA−TRZ** shows virtually no DF. The PF decay from **DMAC−TPA−TRZ** and **DMAC−Ph−TRZ** can be fitted with two exponential decays, i.e., 6.90 ns ([1]CT) and 35.4 ns (dimer), and 18.4 ns ([1]CT) and 73.6 ns (very weak component), respectively. The DF exponential decay of **DMAC−Ph−TPZ** and **DMAC−TPA−TRZ** cannot be fitted reliably.

To determine the lowest-energy [3]LE state of each material, phosphorescence spectra were obtained, as shown in Figure 9b. Phosphorescent emission from **PXZ−TPA−TRZ** cannot be seen even at 20 K, implying that the energy gap between [1]CT and [3]LE is very small and rISC very efficient. The phosphorescence spectra of **DMAC−Ph−TRZ** closely resembled those of the TRZ moiety, indicating this to be the lowest local [3]LE state (E_T = 2.76 eV), whereas, for **PXZ−Ph−TRZ**, the lowest [3]LE state originates from the PXZ, as seen in Figure S18. We also determined the triplet state of the TPA/TRZ dimer (1%) in a zeonex matrix. Indeed, the dimer has triplet energy ([3]DE) at 3.06 eV, while the **DMAC−TPA−TRZ** has an [3]LE of 2.76 eV, as shown in Figure 9b. The [3]DE spectrum is clearly not a superposition of [3]LE states of TRZ and TPA (Figure S19). Hence, the dimer (conformer 2) is expected to display no TADF behavior. In solution, the molecules can transform from one conformer to another; thus, the emission from the DMAC−TRZ CT state will be quenched rapidly by the TPA−TRZ dimer state, as can be seen in Figure 4a,b. As temperature decreases, the viscosity of the solvent increases, increasing the energy barrier for large reorganization required for the dimer to form, so reducing the quenching of the TPA−TRZ CT state, giving rise to weak TADF behavior that can be seen in Figure 4d.[40] In a restricted space such as in a zeonex matrix, the large reorganization required by conformer 2 is significantly suppressed, resulting in
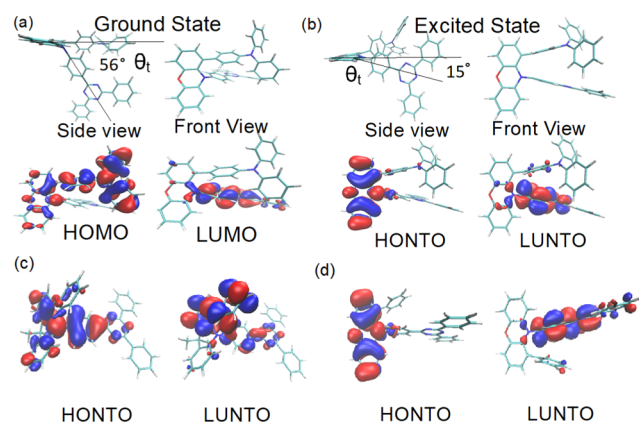

Figure 8. (a) DFT-optimized ground-state geometry of **PXZ−TPA−TRZ** and the frontier orbitals, (b) adiabatic geometry of **PXZ−TPA−TRZ** and the HONTO and LUNTO of the lowest vertical fluorescence. HONTO and LUNTO of vertical fluorescence for (c) **DMAC−Ph−TRZ** and (d) **PXZ−Ph−TRZ**.
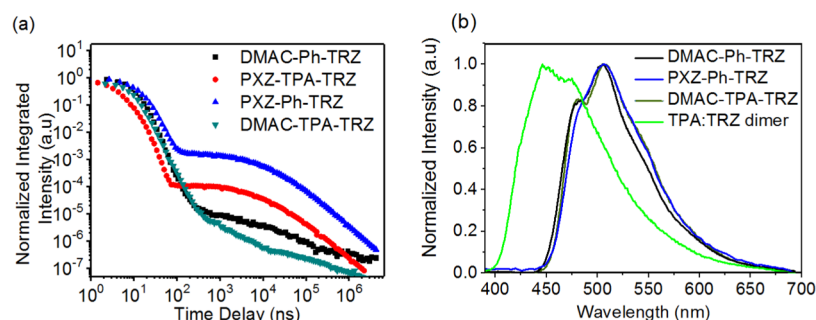
Figure 9. (a) Room-temperature time-resolved fluorescence decay curves in zeonex host and (d) phosphorescence spectra at 80 K for the compounds under study.
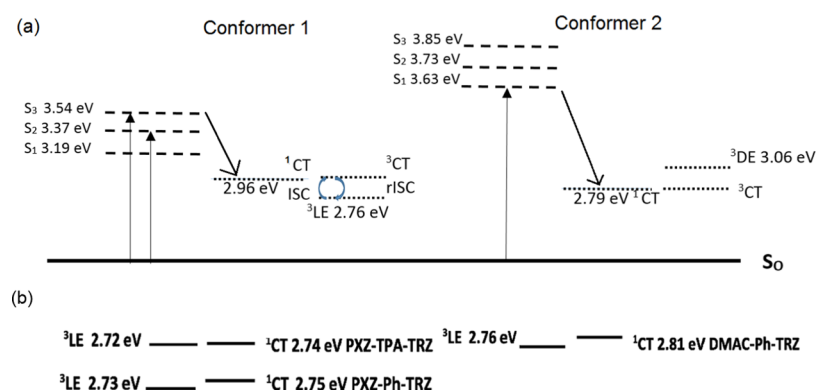

Figure 10. Jablonski diagram for **DMAC−TPA−TRZ** for conformers 1 and 2 and (b) energy levels of the materials **PXZ−TPA−TRZ**, **PXZ−Ph−TRZ**, and **DMAC−Ph−TRZ**.

emission dominated by conformer 1, which has a gap between ^{3}CT and ^{3}LE of 0.2 eV, giving rise to weak TADF. The detailed Jablonski diagrams for **DMAC−TPA−TRZ** along with the summarized relevant energy levels of the materials for **DMAC−TPA−TRZ**, **PXZ−TPA−TRZ**, **DMAC−Ph−TRZ**, and **PXZ−Ph−TRZ** are given in Figure 10.

These materials clearly indicate that conformational states play a crucial role in rISC and TADF processes. From the photophysics of **DMAC−Ph−TRZ**, it exhibits a weak CT state having strong ^{1}LE character. Upon incorporating TPA, two new states are created, a TPA−TRZ CT state and as a result of strong dipole−dipole attraction between TPA and TRZ, a ground-state cofacial dimeric species having a partial through-space CT character. These two states are also identified in theoretical calculations as **DMAC−TPA−TRZ** conformers 1 and 2. From PLE measurements, it is clear though that in the **DMAC−TPA−TRZ** molecule, the dimer state formation is activated by excess energy to overcome the stiffness of the DMAC. This dimeric state, however, has a high-energy local triplet state that quenches DF emission. Thus, the use of asymmetric donors (or acceptors) in a potential TADF molecular design has to be made with care to avoid this possibility of excited-state reorganization driven by dimer/exciplex forces between D and A. Interactions of this sort can be hindered by a rigid bridging moiety such as PXZ or increasing the intramolecular distance between donor and acceptor moieties.

To study the effects of the possible TPA−TRZ excited state in **DMAC−TPA−TRZ**-based devices, all of these compounds were made into OLED devices to measure their electroluminescent (EL) properties. This was achieved through using a common device architecture of glass substrate/indium tin oxide anode/MoO$_3$ (1 nm)/TAPC (40−50 nm)/mCP (10 nm)/mCPCN doped with TADF dopants (8 wt %; 20 nm)/3TPYMB (50−55 nm)/LiF (1 nm)/Al (100 nm). Thermogravimetric (Figure S20) and differential scanning calorimetry (Figure S21) analyses were conducted to probe the thermal and morphological properties of **DMAC−TPA−TRZ**, **DMAC−Ph−TRZ**, **PXZ−TPA−TRZ**, and **PXZ−Ph−TRZ**. In addition, cyclic voltammetry (Figure S22) was employed to study the electrochemical property and determine the HOMO/LUMO energy levels. These data were summarized in Table S4. **DMAC−TPA−TRZ**-, **DMAC−Ph−TRZ**-, **PXZ−TPA−TRZ**-, and **PXZ−Ph−TRZ**-doped mCPCN films exhibit photoluminescence quantum yields (PLQYs) of 50, 45.3, ∼100, and ∼100%, respectively. The lower PLQY for **DMAC−Ph−TRZ** compared to **PXZ−Ph−TRZ** could be the result of an increased nonradiative loss channel due to a larger ^{3}CT and ^{3}LE gap, which reduces the TADF behavior. EL characteristics of OLEDs incorporating these emitters are shown in Figure 11a−d, with their EL performance parameters being summarized in Table 1. The EL spectra, ranging from deep blue to green emission, are similar to corresponding PL spectra in both solution and doped films except **DMAC−TPA−TRZ**. In the latter, in line with the early-time emission measured in zeonex film, a substantial contribution of the emission comes from the dimeric TPA−TRZ excited state, Figure 11a, along with a contribution from the DMAC−TRZ CT state at ca. 480 nm, i.e., on the blue edge of the EL, as well. The EL is very different compared to **DMAC−Ph−TRZ**. The effect of the different host material, mCPCN, is shown in Figures S23 and S24, and data are summarized in Table S5. It can be seen that the PL spectra in mCPCN and zeonex are very similar as well. This is in fact in line with other TADF
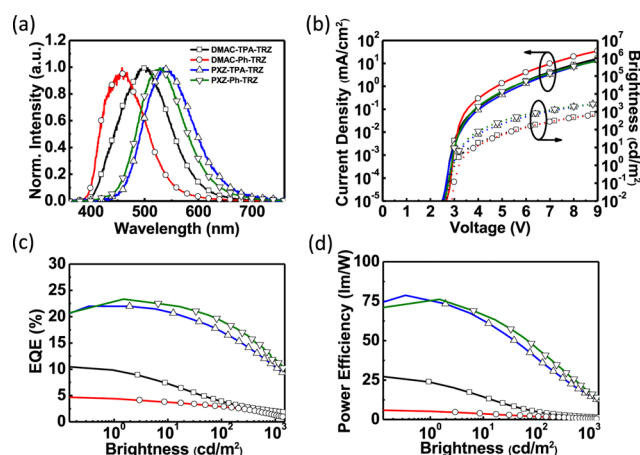
Figure 11. (a) EL spectra, (b) $I-V-L$ characteristics, (c) EQEs, and (d) luminous efficiencies for OLEDs adopting different emitters.

emitters because in dense film, "solid-state solvatochromism" is not possible[43,44] because the host material cannot reorganize around the excited guest molecule to stabilize the excited-state dipole. Thus, the dimer state plays a critical role in the device performance of the **DMAC−TPA−TRZ**-based devices, along with the large singlet−triplet gap. The devices in general exhibit a relatively low turn-on voltage of ∼2.5 V and low operation voltage. Under a similar device architecture, devices adopting high-PLQY emitters **PXZ−TPA−TRZ** and **PXZ− Ph−TRZ** exhibit rather high external quantum efficiencies (EQEs) of up to ∼22−23.3%, while emitters **DMAC−TPA− TRZ** and **DMAC−Ph−TRZ** having lower PLQYs give inferior EQEs of 10.5 and 4.7%, respectively. Noticeably, emitters showing the most pronounced TADF characteristics (i.e., **PXZ−TPA−TRZ** and **PXZ−Ph−TRZ**) give significantly higher EL efficiencies of up to (22%, 70.2 cd A^{-1}, 78.8 lm W^{-1}) and (23.3%, 72.8 cd A^{-1}, 76.2 lm W^{-1}), respectively. On the other hand, **DMAC−TPA−TRZ** (that show less pronounced TADF characteristics) exhibit a lower PLQY of 50% and a lower EQE of 10.5%. Finally, although the device based on blue emitter **DMAC−Ph−TRZ** gives a lower EQE of 4.7% due to its relatively low PLQY of 45.3%, such an EQE indeed is still significantly higher than one would expect from a pure fluorescent emitter of similar PLQY.[45] This suggests a contribution from DF in the EL process even in this compound.

3. CONCLUSIONS

In summary, we developed asymmetrical donor−donor′− acceptors as novel TADF emitters. We show that multiple emission observed in **DMAC−TPA−TRZ** is the result of two distinct TPA−TRZ conformers and a DMAC−TRZ CT state. Due to the flexibility of sp^3 carbon bond in DMAC, excited-state conformational relaxation driven by strong TPA−TRZ

dipole−dipole attraction results in the formation of an intramolecular dimer that gives rise to weak through-space charge transfer, in stark contrast to the rigid PXZ, which prevents these states forming in **PXZ−TPA−TRZ**. This intramolecular dimer state, however, has a high-energy local triplet state that prevents DF, as the singlet−triplet gap (>0.2 eV) is too large to support rISC. By using the more rigid PXZ donor as a bridge, which prevents the dimeric conformation, strong TADF from the PXZ−TRZ CT state yields excellent OLED performance with EQE as high as 23%. Thus, we show that the flexibility of D−A bridging units is very important in emitter design, allowing multiple CT excited states to form. We also find that where strong dipole−dipole attraction between D and A units exists, stable intramolecular dimer species can form (formation may be activated when large molecular reorganization is required), and although such cofacial dimer states can facilitate through-space charge transfer, care must also be taken because the local triplet states of these dimeric species can be rather higher than expected, leading to quenching of rISC because the local triplet cannot easily couple to the dimer CT states.

■ ASSOCIATED CONTENT

Ⓢ Supporting Information

The Supporting Information is available free of charge on the ACS Publications website at DOI: 10.1021/acs.jpcc.9b01900.

> Synthesis, NMR analysis, X-ray structures, thermal properties, and cyclic voltammetry, of new materials, steady-state and time-resolved optical spectroscopy results, theoretical modeling and OLED device fabrication (PDF)

■ AUTHOR INFORMATION

Corresponding Authors
*E-mail: ph7klw76@um.edu.my (K.-L.W.).
*E-mail: wucc@ntu.edu.tw (C.-C.W.).
*E-mail: kenwong@ntu.edu.tw (K.-T.W.).
*E-mail: a.p.monkman@durham.ac.uk (A.P.M.).

ORCID Ⓘ
Marc K. Etherington: 0000-0003-2101-5757
Ken-Tsung Wong: 0000-0002-1680-6186
Andrew P. Monkman: 0000-0002-0784-8640

Notes
The authors declare no competing financial interest.

Table 1. Summary of OLED Characteristics of Various Compounds

emitter	η_{ext}[a] (%) max., 100, 1000 cd m^{-2}	η_c[b] (cd A^{-1}) max., 100, 1000 cd m^{-2}	η_p[c] (lm W^{-1}) max., 100, 1000 cd m^{-2}	CIE[d]	φ (%)
DMAC−TPA−TRZ	10.5, 3.8, 2.1	24.2, 8.8, 4.6	27.2, 5.1, 1.9	(0.20, 0.35)	50
DMAC−Ph−TRZ	4.7, 2.9, 1.2	5.6, 3.5, 1.5	5.9, 1.9, 0.5	(0.16, 0.16)	45.3
PXZ−TPA−TRZ	22.0, 17.1, 10.6	70.2, 54.9, 33.2	78.8, 39.5, 15.7	(0.35, 0.54)	100
PXZ−Ph−TRZ	23.3, 19.3, 12.0	72.8, 59.8, 36.6	76.2, 45.3, 18.0	(0.30, 0.53)	100

[a]External quantum efficiency. [b]Current efficiency. [c]Power efficiency. [d]1931 Commission Internationale de l'Eclairage (CIE) coordinates.

■ REFERENCES

(1) Santos, P. L.; Ward, J. S.; Data, P.; Batsanov, A.; Bryce, M. R.; Dias, F.; Monkman, A. P. Engineering the Singlet-Triplet Energy Splitting in a TADF Molecule. *J. Mater. Chem. C* **2016**, *4*, 3815−3824.

(2) Etherington, M. K.; Gibson, J.; Higginbotham, H. F.; Penfold, T. J.; Monkman, A. P. Revealing the Spin-Vibronic Coupling Mechanism of Thermally Activated Delayed Fluorescence. *Nat. Commun.* **2016**, *7*, No. 13680.

(3) Gibson, J.; Monkman, A. P. A. P.; Penfold, T. J. T. J. The Importance of Vibronic Coupling for Efficient Reverse Intersystem Crossing in Thermally Activated Delayed Fluorescence Molecules. *ChemPhysChem* **2016**, *17*, 2956−2961.

(4) Gibson, J.; Penfold, T. J. Nonadiabatic Coupling Reduces the Activation Energy in Thermally Activated Delayed Fluorescence. *Phys. Chem. Chem. Phys.* **2017**, *19*, 8428−8434.

(5) Dias, F. B.; Penfold, T. J.; Monkman, A. P. Photophysics of Thermally Activated Delayed Fluorescence Molecules. *Methods Appl. Fluoresc.* **2017**, *5*, No. 012001.

(6) Im, Y.; Kim, M.; Cho, Y. J.; Seo, J.-A.; Yook, K. S.; Lee, J. Y. Molecular Design Strategy of Organic Thermally Activated Delayed Fluorescence Emitters. *Chem. Mater.* **2017**, *29*, 1946−1963.

(7) Chen, X.-K.; Kim, D.; Brédas, J.-L. Thermally Activated Delayed Fluorescence (TADF) Path toward Efficient Electroluminescence in Purely Organic Materials: Molecular Level Insight. *Acc. Chem. Res.* **2018**, *51*, 2215−2224.

(8) Zhang, M.-Y.; Li, Z.-Y.; Lu, B.; Wang, Y.; Ma, Y.-D.; Zhao, C.-H. Solid-State Emissive Triarylborane-Based [2.2]Paracyclophanes Displaying Circularly Polarized Luminescence and Thermally Activated Delayed Fluorescence. *Org. Lett.* **2018**, *20*, 6868−6871.

(9) Kawasumi, K.; Wu, T.; Zhu, T.; Chae, H. S.; Van Voorhis, T.; Baldo, M. A.; Swager, T. M. Thermally Activated Delayed Fluorescence Materials Based on Homoconjugation Effect of Donor−Acceptor Triptycenes. *J. Am. Chem. Soc.* **2015**, *137*, 11908−11911.

(10) Tsujimoto, H.; Ha, D. G.; Markopoulos, G.; Chae, H. S.; Baldo, M. A.; Swager, T. M. Thermally Activated Delayed Fluorescence and Aggregation Induced Emission with Through-Space Charge Transfer. *J. Am. Chem. Soc.* **2017**, *139*, 4894−4900.

(11) Ren, Z.; Nobuyasu, R. S.; Dias, F. B.; Monkman, A. P.; Yan, S.; Bryce, M. R. Pendant Homopolymer and Copolymers as Solution-Processable Thermally Activated Delayed Fluorescence Materials for Organic Light-Emitting Diodes. *Macromolecules* **2016**, *49*, 5452−5460.

(12) Shao, S. Y.; Hu, J.; Wang, X. D.; Wang, L. X.; Jing, X. B.; Wang, F. S. Blue Thermally Activated Delayed Fluorescence Polymers with Nonconjugated Backbone and Through-Space Charge Transfer Effect. *J. Am. Chem. Soc.* **2017**, *139*, 17739−17742.

(13) He, Z. Z.; Cai, X. Y.; Wang, Z. H.; Li, Y. C.; Xu, Z. D.; Liu, K. K.; Chen, D. C.; Su, S. J. Sky-Blue Thermally Activated Delayed Fluorescence Material Employing a Diphenylethyne Acceptor for Organic Light-Emitting Diodes. *J. Mater. Chem. C* **2018**, *6*, 36−42.

(14) Yu, L.; Wu, Z. B.; Xie, G. H.; Zeng, W. X.; Ma, D. G.; Yang, C. L. Molecular Design to Regulate the Photophysical Properties of Multifunctional TADF Emitters towards High-Performance TADF-Based OLEDs with EQEs up to 22.4% and Small Efficiency Roll-Offs. *Chem. Sci.* **2018**, *9*, 1385−1391.

(15) Zhang, Y. G.; Zhang, D. D.; Cai, M. H.; Li, Y. L.; Zhang, D. Q.; Qiu, Y.; Duan, L. Towards Highly Efficient Red Thermally Activated Delayed Fluorescence Materials by the Control of Intra-Molecular Pi-Pi Stacking Interactions. *Nanotechnology* **2016**, *27*, No. 094001.

(16) Wu, J.-Y.; Chen, S.-A. Development of a Highly Efficient Hybrid White Organic-Light-Emitting Diode with a Single Emission Layer by Solution Processing. *ACS Appl. Mater. Interfaces* **2018**, *10*, 4851−4859.

(17) Tsai, W.-L.; Huang, M.-H.; Lee, W.-K.; Hsu, Y.-J.; Pan, K.-C.; Hung, Y.-H.; Ting, H.-C.; Sarma, M.; Ho, Y.-Y.; Hu, H.-C.; Chen, C.-C.; Lee, M.-T.; Wong, K.-T.; Wu, C.-C. A versatile thermally activated delayed fluorescence emitter for both highly efficient doped and non-doped organic light emitting devices. *Chem. Commun.* **2015**, *51*, 13662−13665.

(18) Pan, K.-C.; Li, S.-W.; Ho, Y.-Y.; Shiu, Y.-J.; Tsai, W.-L.; Jiao, M.; Lee, W.-K.; Wu, C.-C.; Chatterjee, T.; Li, Y.-S.; Wong, K.-T.; Hu, H.-C.; Chen, C.-C.; Lee, M.-T.; Lee, M.-T. Efficient and Tunable Thermally Activated Delayed Fluorescence Emitters Having Orientation Adjustable CN Substituted Pyridine and Pyrimidine Acceptor Units. *Adv. Funct. Mater.* **2016**, *26*, 7560−7571.

(19) Aydemir, M.; Xu, S.; Chen, C.; Bryce, M. R.; Chi, Z.; Monkman, A. P. Photophysics of an Asymmetric Donor-Acceptor-Donor′ TADF Molecule and Reinterpretation of Aggregation-Induced TADF Emission in These Materials. *J. Phys. Chem. C* **2017**, *121*, 17764−17772.

(20) Higginbotham, H. F.; Yi, C.-L.; Monkman, A. P.; Wong, K.-T. Effects of Ortho-Phenyl Substitution on the rISC Rate of D−A Type TADF Molecules. *J. Phys. Chem. C* **2018**, *122*, 7627−7634.

(21) Penfold, T. J.; Dias, F. B.; Monkman, A. P. The Theory of Thermally Activated Delayed Fluorescence for Organic Light Emitting Diodes. *Chem. Commun.* **2018**, *54*, 3926−3935.

(22) Higginbotham, H. F.; Yi, C.-L.; Monkman, A. P.; Wong, K.-T. Effects of Ortho-Phenyl Substitution on the rISC Rate of D−A Type TADF Molecules. *J. Phys. Chem. C* **2018**, *122*, 7627−7634.

(23) Tanaka, H.; Shizu, K.; Nakanotani, H.; Adachi, C. Dual Intramolecular Charge-Transfer Fluorescence Derived from a Phenothiazine-Triphenyltriazine Derivative. *J. Phys. Chem. C* **2014**, *118*, 15985−15994.

(24) Etherington, M. K.; Franchello, F.; Gibson, J.; Northey, T.; Santos, J.; Ward, J. S.; Higginbotham, H. F.; Data, P.; Kurowska, A.; Dos Santos, P. L.; et al. Regio- and Conformational Isomerization Critical to Design of Efficient Thermally-Activated Delayed Fluorescence Emitters. *Nat. Commun.* **2017**, *8*, No. 14987.

(25) Aydemir, M.; Haykir, G.; Türksoy, F.; Gümüş, S.; Dias, F. B.; Monkman, A. P. Synthesis and Investigation of Intra-Molecular Charge Transfer State Properties of Novel Donor-Acceptor-Donor Pyridine Derivatives: The Effects of Temperature and Environment on Molecular Configurations and the Origin of Delayed Fluorescence. *Phys. Chem. Chem. Phys.* **2015**, *17*, 25572−25582.

(26) Jankus, V.; Monkman, A. P. Is Poly(Vinylcarbazole) a Good Host for Blue Phosphorescent Dopants in PLEDs? Dimer Formation and Their Effects on the Triplet Energy Level of Poly(N-Vinylcarbazole) and Poly(N-Ethyl-2-Vinylcarbazole). *Adv. Funct. Mater.* **2011**, *21*, 3350−3356.

(27) dos Santos, P. L.; Etherington, M. K.; Monkman, A. P. Chemical and Conformational Control of the Energy Gaps Involved in the Thermally Activated Delayed Fluorescence Mechanism. *J. Mater. Chem. C* **2018**, *6*, 4842−4853.

(28) dos Santos, P. L.; Ward, J. S.; Batsanov, A. S.; Bryce, M. R.; Monkman, A. P. Optical and Polarity Control of Donor Acceptor Conformation and Their Charge-Transfer States in Thermally Activated Delayed Fluorescence Molecules. *J. Phys. Chem. C* **2017**, *121*, 16462−16469.

(29) Wang, K.; Zheng, C.-J.; Liu, W.; Liang, K.; Shi, Y.-Z.; Tao, S.-L.; Lee, C.-S.; Ou, X.-M.; Zhang, X.-H. Avoiding Energy Loss on TADF Emitters: Controlling the Dual Conformations of D-A Structure Molecules Based on the Pseudoplanar Segments. *Adv. Mater.* **2017**, *29*, No. 1701476.

(30) Dias, F. B.; Santos, J.; Graves, D. R.; Data, P.; Nobuyasu, R. S.; Fox, M. A.; Batsanov, A. S.; Palmeira, T.; Berberan-Santos, M. N.; Bryce, M. R.; et al. The Role of Local Triplet Excited States and D-A Relative Orientation in Thermally Activated Delayed Fluorescence: Photophysics and Devices. *Adv. Sci.* **2016**, *3*, No. 1600080.

(31) Northey, T.; Stacey, J.; Penfold, T. J. The Role of Solid State Solvation on the Charge Transfer State of a Thermally Activated

Delayed Fluorescence Emitter. *J. Mater. Chem. C* **2017**, *5*, 11001−11009.

(32) Sun, H. T.; Zhong, C.; Bredas, J. L. Reliable Prediction with Tuned Range-Separated Functionals of the Singlet-Triplet Gap in Organic Emitters for Thermally Activated Delayed Fluorescence. *J. Chem. Theory Comput.* **2015**, *11*, 3851−3858.

(33) Körzdörfer, T.; Bredas, J. L. Organic Electronic Materials: Recent Advances in the DFT Description of the Ground and Excited States Using Tuned Range-Separated Hybrid Functionals. *Acc. Chem. Res.* **2014**, *47*, 3284−3291.

(34) Chen, D.-G.; Lin, T.-C.; Chen, Y.-A.; Chen, Y.-H.; Lin, T.-C.; Chen, Y.-T.; Chou, P. T. Revisiting Dual Intramolecular Charge-Transfer Fluorescence of Phenothiazine-Triphenyltriazine Derivatives. *J. Phys. Chem. C* **2018**, *122*, 12215−12221.

(35) Lee, K.; Kim, D. Local-Excitation versus Charge-Transfer Characters in the Triplet State: Theoretical Insight into the Singlet−Triplet Energy Differences of Carbazolyl-Phthalonitrile-Based Thermally Activated Delayed Fluorescence Materials. *J. Phys. Chem. C* **2016**, *120*, 28330−28336.

(36) dos Santos, P. L.; Dias, F. B.; Monkman, A. P. Investigation of the Mechanisms Giving Rise to TADF in Exciplex States. *J. Phys. Chem. C* **2016**, *120*, 18259−18267.

(37) Mataga, N.; Chosrowjan, H.; Taniguchi, S. Ultrafast Charge Transfer in Excited Electronic States and Investigations into Fundamental Problems of Exciplex Chemistry: Our Early Studies and Recent Developments. *J. Photochem. Photobiol., C* **2005**, *6*, 37−79.

(38) Moon, C.-K.; Huh, J.-S.; Kim, J.-M.; Kim, J.-J. Electronic Structure and Emission Process of Excited Charge Transfer States in Solids. *Chem. Mater.* **2018**, *30*, 5648−5654.

(39) Dias, F. B.; King, S.; Monkman, A. P.; Perepichka, I. I.; Kryuchkov, M. A.; Perepichka, I. F.; Bryce, M. R. Dipolar Stabilization of Emissive Singlet Charge Transfer Excited States in Polyfluorene Copolymers. *J. Phys. Chem. B* **2008**, *112*, 6557−6566.

(40) Wasielewski, M. R.; Johnson, D. G.; Niemczyk, M. P.; Gaines, G. L.; O'Neil, M. P.; Svec, W. A. Chlorophyll-Porphyrin Heterodimers with Orthogonal.Pi. Systems: Solvent Polarity Dependent Photophysics. *J. Am. Chem. Soc.* **1990**, *112*, 6482−6488.

(41) Johnson, E. R.; Keinan, S.; Mori-Sánchez, P.; Contreras-García, J.; Cohen, A. J.; Yang, W. Revealing Noncovalent Interactions. *J. Am. Chem. Soc.* **2010**, *132*, 6498−6506.

(42) Ye, J.-T.; Wang, L.; Wang, H.-Q.; Pan, X.-M.; Xie, H.-M.; Qiu, Y.-Q. Effective Impact of Dielectric Constant on Thermally Activated Delayed Fluorescence and Nonlinear Optical Properties: Through-Bond/-Space Charge Transfer Architectures. *J. Phys. Chem. C* **2018**, *122*, 18850−18859.

(43) Etherington, M. K.; Kukhta, N. A.; Higginbotham, H. F.; Danos, A.; Bismillah, A. N.; Graves, D. R.; McGonigal, P. R.; Haase, N.; Morherr, A.; Batsanov, A. S.; et al. Persistent Dimer Emission in Thermally Activated Delayed Fluorescence Materials. *J. Phys. Chem. C* **2019**, DOI: 10.1021/acs.jpcc.9b01458.

(44) Northey, T.; Stacey, J.; Penfold, T. J. The Role of Solid State Solvation on the Charge Transfer State of a Thermally Activated Delayed Fluorescence Emitter. *J. Mater. Chem. C* **2017**, *5*, 11001−11009.

(45) Endo, A.; Sato, K.; Yoshimura, K.; Kai, T.; Kawada, A.; Miyazaki, H.; Adachi, C. Efficient Up-Conversion of Triplet Excitons into a Singlet State and Its Application for Organic Light Emitting Diodes. *Appl. Phys. Lett.* **2011**, *98*, No. 083302.